

NUMERICAL AND EXPERIMENTAL STUDY OF THE EFFECT OF ARTIFICIAL POROSITY IN A LATTICE STRUCTURE MANUFACTURED BY LASER BASED POWDER BED FUSION

Anton du Plessis ¹, Ina Yadroitsava ², Dean Kouprianoff ², Igor Yadroitsev ²

¹ CT Scanner Facility and Physics Department, Stellenbosch University, Stellenbosch, South Africa 7602

² Department of Mechanical Engineering, Central University of Technology, Bloemfontein, South Africa 9301

Abstract

Additively manufactured lattice structures are used in various applications due to their unique properties, especially low weight with relatively good strength and stiffness. While lattices have been investigated widely, the effect of manufacturing flaws on the lattice performance was not yet analyzed in detail. One important type of manufacturing flaw which can be relatively easily analyzed numerically and experimentally is unwanted voids or porosity. In this work, using a simple cubic lattice structure as a test case, pores with varying sizes were induced in a single strut and compressive loading simulated. Ti6Al4V ELI (extra low interstitial) lattices produced by laser powder bed fusion, with and without induced pores, were subjected to mechanical compression tests. MicroCT images validated the presence and size of the induced voids in produced samples. The mechanical compression results show that even relatively large pores in individual load-bearing struts do not affect the ultimate compressive strength of these particular lattice shapes studied and for individual large pores.

Introduction

Lattice structures built by additive manufacturing (AM) are suitable for various applications where light weight is required while maintaining reasonable strength and stiffness. One of the major applications is in bone replacement implants, due to the ability to tailor the effective Young's Modulus to match that of bone, and simultaneously allowing the flow of nutrients and cell growth on the structure and eventually allow bone ingrowth into the porous scaffold structure. Recent reviews of lattice structures for bone replacement implants discuss these requirements in more detail [1]–[4]. The mechanical properties of lattice structures can, in general, be predicted with reasonable accuracy through the Ashby-Gibson model, which is a simplified model for open cell foams [5], [6]. Most importantly, the Young's modulus and yield stress are predicted as a function of density. Generally lattice structures can be designed with a target pore size and total porosity: for bone replacement implants in Ti6Al4V, a Young's modulus in the region of 20 GPa is typically desired to match that of cortical bone [1], which translates to a porosity of ~60%.

As evidenced by the Ashby-Gibson model, mechanical properties of lattice structures are mainly influenced by relative density. In turn, relative density is a function of strut thickness and spacing, for a given unit cell shape. Parthasarathy *et al.* [7] investigated electron beam melted Ti6Al4V samples – four designs of cubic-type cells with different relative densities were investigated and it was found that the Young's modulus and compressive strength of the built

samples are lower than that predicted by the Ashby-Gibson model, and especially low for the thinnest strut version. This might indicate limitations of AM, *i.e.* build inaccuracies which are more detrimental to thinner structures and cause premature failure in the thinnest struts in lattices, mainly due to geometrical inaccuracy. Similar designs were produced by Laser based powder bed fusion (LPBF) and compared to the above results [8]. Especially interesting in this latter work is that parts with internal defects (non-intentional pores) produced by using excessive volumetric energy density input, showed high mechanical properties when experimental relative density is taken into account. In fact, considering the reduced total density due to these pores, these as-built parts were relatively stronger than the parts with less internal defects. This was partially attributed to different nitrogen and oxygen contents in the material. Other reason can be linked with relaxation/re-distribution of residual stress in porous as-built LPBF material after separating from the substrate. In a different study of the influence of porosity on mechanical properties of solid additively manufactured Ti6Al4V, it was found that small pores with total volume fraction up to 1% have no effect on mechanical properties, but larger pores with volume fraction around 5% cause major loss of mechanical properties [9]. This indicates that small pores may be harmless, but the exact threshold for this size is not yet clear. Furthermore, lattice structures comprise typically of thin struts only a few times wider than the pore itself, so it is not clear whether this rule about “harmless small pores” is equally applicable to lattice structures, as it is with larger parts.

Finite element modelling (FEM) can be used to analyze the deformation and stress distributions in lattice structures, and for interpreting failure mechanisms, especially in combination with experimental data [10]. The method has been used to compare lattices comprising of different unit cell designs such as rhombic and octet [11], rhombic and diagonal [12], topology optimized lattice structures [13] and even single struts [14]. FEM finds particular application when new lattice designs are investigated [15] or when different designs are compared [16]–[18], as it offers a practical means of evaluating designs without the expense and time involved in production of prototype structures. Recently, imperfections caused by additive manufacturing have been incorporated into FEM models using statistically varying strut thickness and strut porosity, with resulting stiffness corresponding well to experimental data [19]. This promising approach allows an improved understanding of the effects of manufacturing imperfections on the mechanical properties of lattice structures, but it remains an idealized model-based method.

In this work, a simplified FEM method was used to investigate the effect of isolated LPBF defects on the maximum local stress concentrations due to compressive loading. We introduce a spherical defect of varying size in a single strut of a lattice structure. The maximum stresses are measured at the defect edge and the adjacent strut. Since real defects in additive manufactured parts can often have sharp edges, a square defect rotated by 45° relative to loading direction is also introduced for comparison. Typical pore defect morphology in real additive manufactured solid Ti6Al4V samples are far smaller and less sharp [20], [21], that means these simulations are a “worst case scenario”. A similar process was used recently to investigate stress concentrators in solid tensile samples, and which showed that the fatigue crack initiation is strongly affected by stress concentrations found by linear elastic simulation [22]. Therefore, the results of the relative stress concentrations found in this study might be important for fatigue properties of lattices as well.

LPBF Ti6Al4V ELI (extra low interstitial) samples with and without artificial defects were manufactured and analyzed by high resolution microCT to confirm the presence of the intentional defects and quantify the maximum defect size, prior to compression testing. The use of microCT

in additive manufacturing has been reviewed recently [23]. The control samples also contained unexpected pores of smaller diameter, and the intentional pores varied in size. This allows for the first quantitative assessment of the influence of pore defect size on the compressive strength of lattice structures. The microCT data is further used for simulations to investigate the differences between stress distributions of an ideal model and the physical sample.

Materials and methods

Regular rectangular lattices were designed in Autodesk Fusion 360. This design was selected as a starting point for this work, partly due to its simplified shape and partly due to the simplicity of designing it without the need for lattice design dedicated software. FEM was performed in a relatively new voxel-based static load simulation (elastic regime) in Volume Graphics VGStudioMax 3.0, the “Structural mechanics simulation” module. This method required the imported .STL format data to be converted to voxel data, after which defects could be simulated by introducing regular-shaped defect “regions of interest” to the voxel data. An identical simulation procedure could subsequently be used for real samples, using microCT voxel data, allowing direct comparison of models and real samples.

The cubic lattice was designed with a total 15 mm width, 0.75 mm strut thickness and 8 struts across one direction in total, resulting in 1.28 mm distance between struts and total 65% porosity. This design is shown in Figure 1(a). In addition to simulations, 12 samples of lattice cube were manufactured by laser based powder bed fusion (LPBF): 4 control samples without artificial pores, 4 samples with designed spherical pores of 0.5 mm diameter and 4 samples with designed cubic pores of roughly the same diameter. The spherical defect was introduced with a region growing tool (as shown in Figure 1(b)); the square defect was introduced with a rectangular region tool and subsequently rotated in one axis by 45°. Load simulations were performed with a nominal 1 kN load and with material parameters set for Ti6Al4V, with Young’s modulus 115 GPa, Poisson’s ratio 0.3 and 32-bit float precision, using simulation cell size of 40 μm across the entire structure.

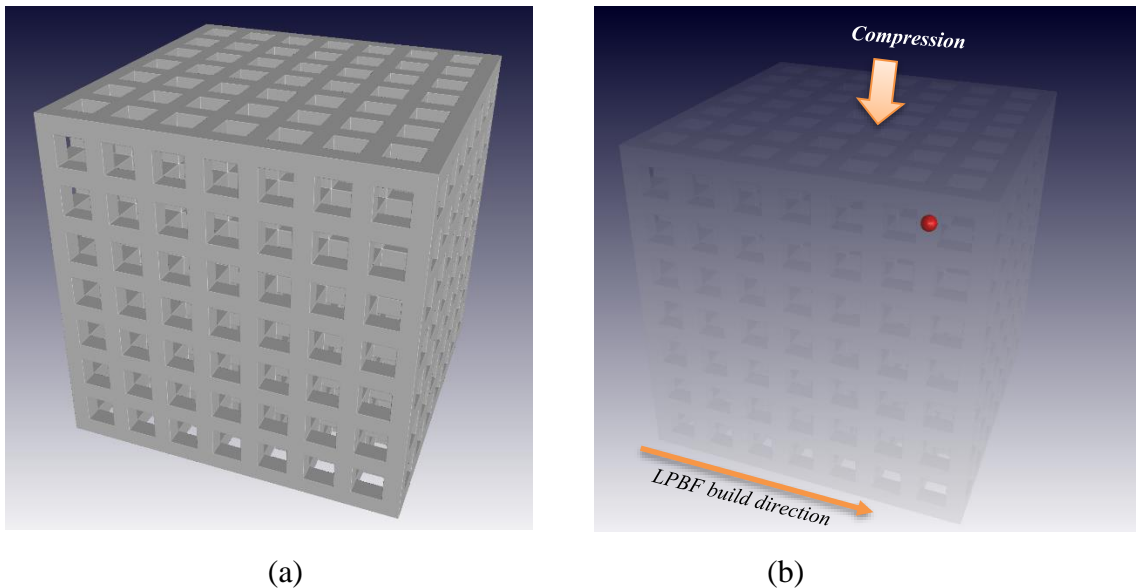


Figure 1: Designed lattice, (a) surface view, (b) intentionally designed spherical pore in transparent view.

The voxel-based simulation in VGStudioMax was recently used to analyze microCT data of castings with defects and correlate physical tensile strength and ductility found by mechanical tests to that of the stresses found by simulation [24]. The same method was applied to a range of samples produced by additive manufacturing, allowing prediction of failure location and force [25]. More recently the method was used to investigate the properties of various designs of a bio-inspired lattice-shell structures for protective applications [26]. A result of the load simulation is shown in Figure 2, with higher stress in the strut containing the designed pore space.

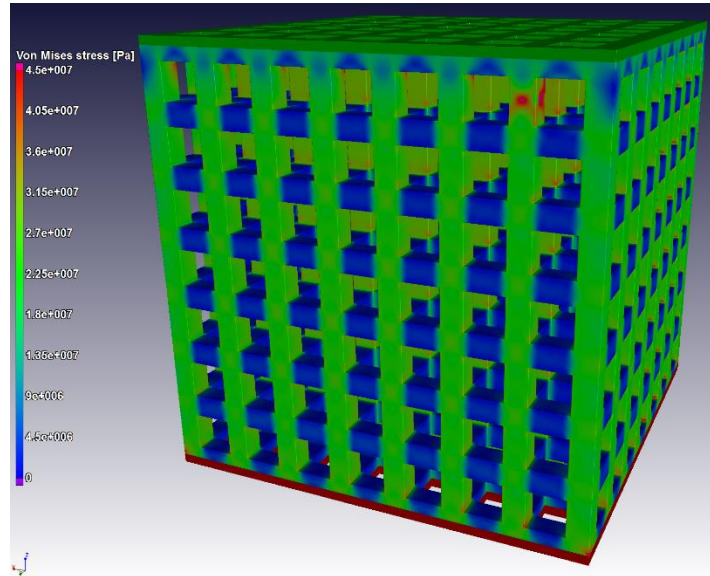


Figure 2: Compressive load simulation (elastic regime) shows higher stresses in vertical struts, and increased stress in the strut containing the pore.

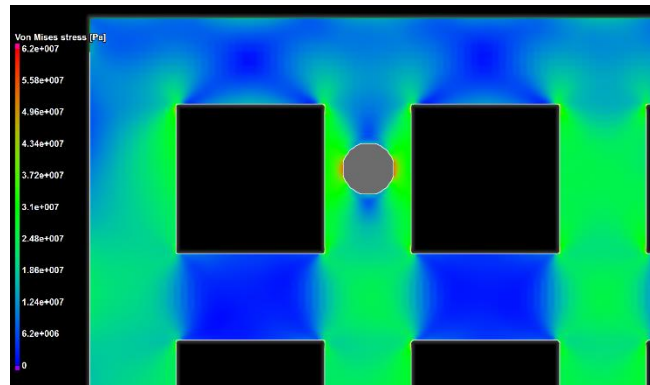
This simulation method allows different resolutions for the simulation cell size, equivalent to mesh size in traditional FEM software, but it makes use of an immersed-boundary FEM code, thereby not requiring a conforming mesh. In this work, local stress values were measured using analysis annotations in the high-stress regions around the introduced defects (maximum value found in region of interest) and in the adjacent strut where no defect occurs, directly to the inside of the structure laterally. A total maximum stress value could also be measured as follows: since each simulation cell size has an associated stress value, the volumetric 1% of cells with highest stress values could be used to provide a mean value of the highest stresses across the entire structure. All simulations were performed on analysis workstations, using multi-core CPUs and 96-128 Gb RAM [27].

Lattice samples were manufacturing using an EOS M280 system. The artificial defects were positioned inside the horizontal struts. Compression tests were therefore done in the direction along the horizontally-built struts (using microCT as validation and orientation (Figure 1b). Stress relieving cycle in Ar atmosphere of 3 hours at 650°C with furnace cooling was carried out before removal from the substrate, ensuring minimal residual stress is present in the parts [20-21]. MicroCT of all samples were done using optimized parameters [28]–[30] followed by compression testing using an Amsler press with 250 kN max.

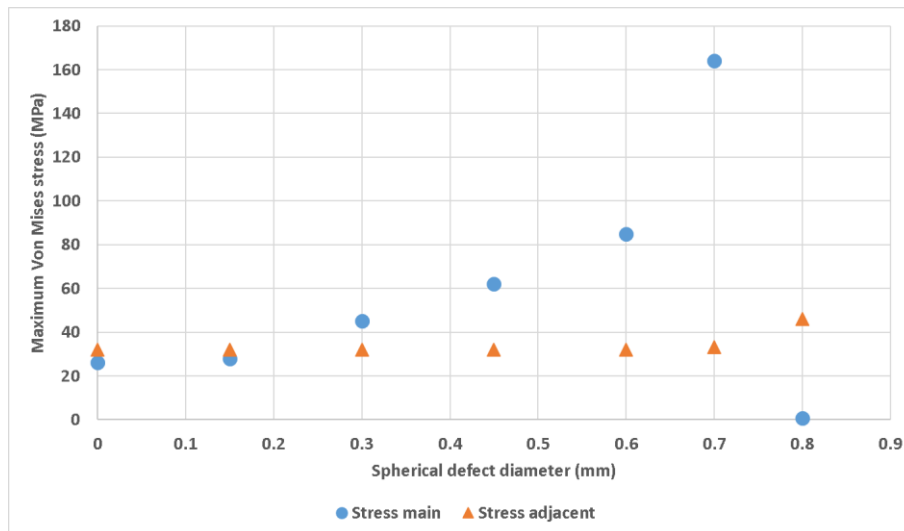
Results and discussion

Simulations on CAD files with intentional pores introduced

Compressive loading simulations were performed on design files to investigate the maximum local stresses in the struts due to varying sizes of spherical pores. By introducing a spherical defect of varying size in the lattice model, the resulting maximum local stress in the strut with the pore and the adjacent strut can be obtained. An example of such a simulation with a spherical pore with 0.45 mm diameter is shown in Figure 3 (a). In this case the adjacent strut where stress is measured locally refers to the vertical strut to the right of the strut with pore space in Figure 3(a). The stresses as a function of pore diameter are shown in Figure 3(b): the measured maximum local stress at the pore, as well as the stress in the middle of the adjacent strut. When the pore size becomes larger than the strut, effectively simulating a failed strut carrying no load, the adjacent strut stress increases substantially. As expected, smaller pores result in lower stresses, with minimal influence at 150 μm .



(a)

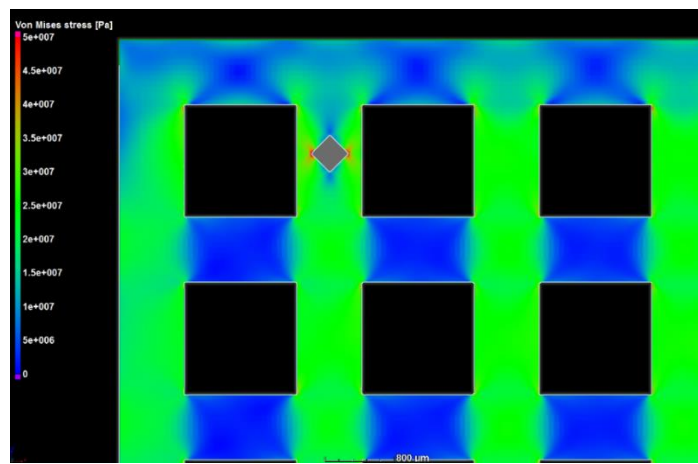


(b)

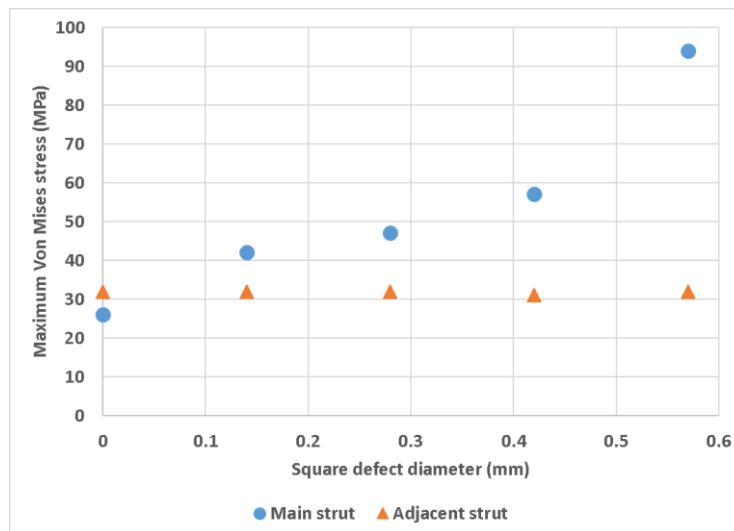
Figure 3: (a) Spherical defect stress distribution shown in slice image for 0.45 mm defect, (b) results of a series of simulations of different spherical defect sizes, showing stress in main strut

where defect is introduced and adjacent strut. Strut diameter was 0.75 mm hence the 0.8 mm defect effectively represents a broken strut.

Most often, under optimal build parameters the typical size range of defects in LPBF Ti6Al4V are in the region of 30-50 μm diameter with roughly spherical geometry [26]. For defects in this range below 50 μm , it seems that the compressive load induced local stress does not significantly increase, when the defects are spherical. However, real defects produced by LPBF are often not spherical or rounded, but elongated in shape [20]. Additive manufactured defects can also sometimes be significantly more irregular as shown in [29] for very planar lack-of-fusion defects. When they are irregular the defects may include sharp edges which act as stress concentrators. In order to simulate this, a cube-shaped defect was introduced instead of a sphere, and turned by 45 degrees relative to the load direction. This is shown in Figure 4(a) with stress distribution obtained from simulations with different-sized cubic defects in Figure 4(b).



(a)



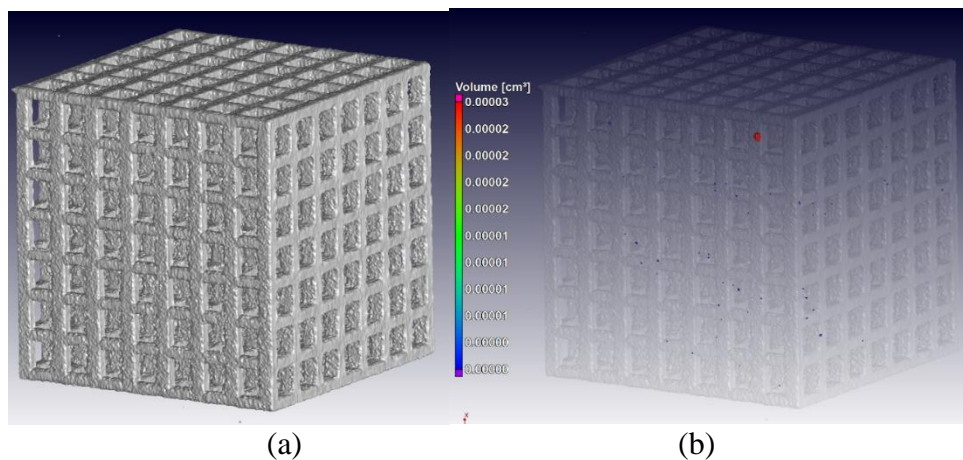
(b)

Figure 4: Slice image of square/cubic defect stress distribution (a) for a square with 400 μm side length, effectively equal to 560 μm maximum cross section perpendicular to load, (b) stress values in main and adjacent strut for different size cubes.

The local von Mises maximum stress was higher in square pore case than for a spherical pore of the same size – *e. g.* for pore diameters of 0.55 mm the stress maximum is about 95 MPa for a square pore but only ~ 75 MPa for a spherical pore. Ideally, all internal defects should be eliminated through optimized build parameters, high quality powder, clean atmosphere and build conditions and additional hot isostatic pressing (HIP) can be used to reduce internal porosity. However, due to the nature of the small features, often defects can be connected to the surface through micro-cracks making the HIP treatment ineffective in near-surface pores [29]. Nevertheless, for typical additive manufactured defect sizes as reported in [29], the stresses are insignificantly small.

Production and microCT analysis of physical models

Physical models were produced in Ti6Al4V with 15 mm side lengths; 4 control samples, 4 with a single artificial spherical pore ~0.5 mm in diameter, and 4 samples with a single cubic pore roughly 0.5 mm in diameter. MicroCT scans were performed on all samples at a voxel size of 25 μm , using 180 kV and 200 μA with 0.5 mm copper beam filtration. Scan parameters were optimized according to the guidelines in [31], one of the spherical-pore samples shown in Figure 5. The pore spaces in all cases did not perfectly match the designed shape exactly and included unmelted powder, which is not expected to contribute significantly to the mechanical properties, relative to empty pore space. This is an assumption which is difficult to test in practice, but considering the presence of powders in typical AM defects, especially large lack of fusion pores, this is a reasonable assumption in this case.



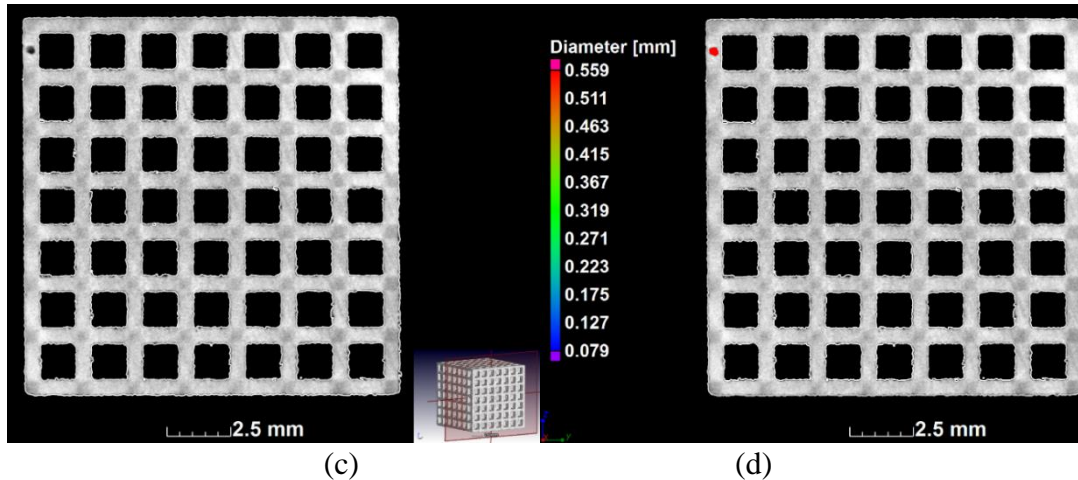
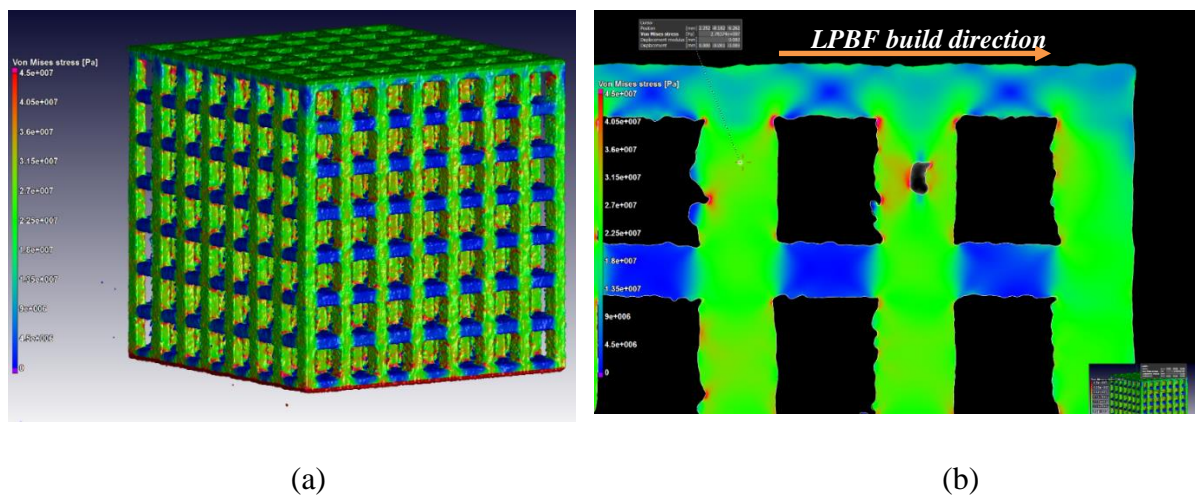
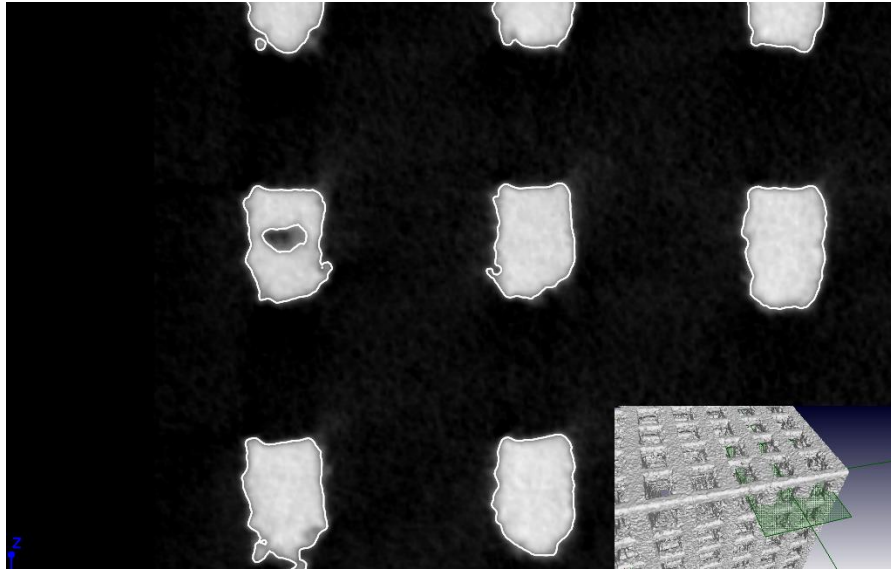


Figure 5: MicroCT validated the presence of intentionally designed pore, (a) shows the surface view, (b) the transparent view with the designed pore space in red, (c) and (d) show the CT slice image without and with analysis colour included.

The microCT data could be used for identical simulations as for designed files, with the aim to highlight differences and see if local stresses at the designed pore is higher due to the rough surface, for example. As shown in Figure 6(a) the stress distribution is similar to the design-file simulations, as expected. The details slice image in Figure 6(b) shows the stress around the designed pore and surprisingly high stress near the surface due to the imperfect surface roughness. In this case the pore is 0.5 mm in its widest axis, but is irregularly shaped, as shown in Figure 6(c) viewed from top. The bottom of the horizontal struts shows high stress concentrations, this is due to the building orientation that is caused by the molten pool not being able to penetrate and attach to previously solidified material. The annotation in Figure 6(b) shows the local stress in the strut adjacent to the strut containing the pore, which is used for comparison with CAD design file simulations.





(c)

Figure 6: Compressive load simulation on microCT data of produced lattice containing intentionally designed spherical pore (a); (b) shows stress around the pore but also at the surface due to roughness. Loading direction is vertical in this image. (c) shows a slice image of the pore from top view, indicating the irregular shape. In this case the widest pore diameter is 0.45 mm and the pore is not perfectly spherical as designed.

In addition to simulations of the CAD file with and without a pore, the real microCT data of this sample could also be simulated with and without the pore space by simple image segmentation (removing the pore virtually as if it becomes part of the material, but leaving everything else unchanged). This comparison is shown in Figure 7(a) for the maximum stress over the entire structure, and in Figure 7(b) for the local stress on the strut adjacent to the strut with pore. This indicates that the cumulative effect of the rough surface has a significant influence on the maximum stress over the whole structure, and also on the local stress in the strut. The maximum stress values are not significantly affected by the presence of the pore – indicating that most of the large stress areas are located elsewhere (in corners and in notches on the surface). There is a slight increase in local stress on the strut adjacent to the pore strut when the pore is included, as expected, and this is a larger increase for the real pore than the designed pore.

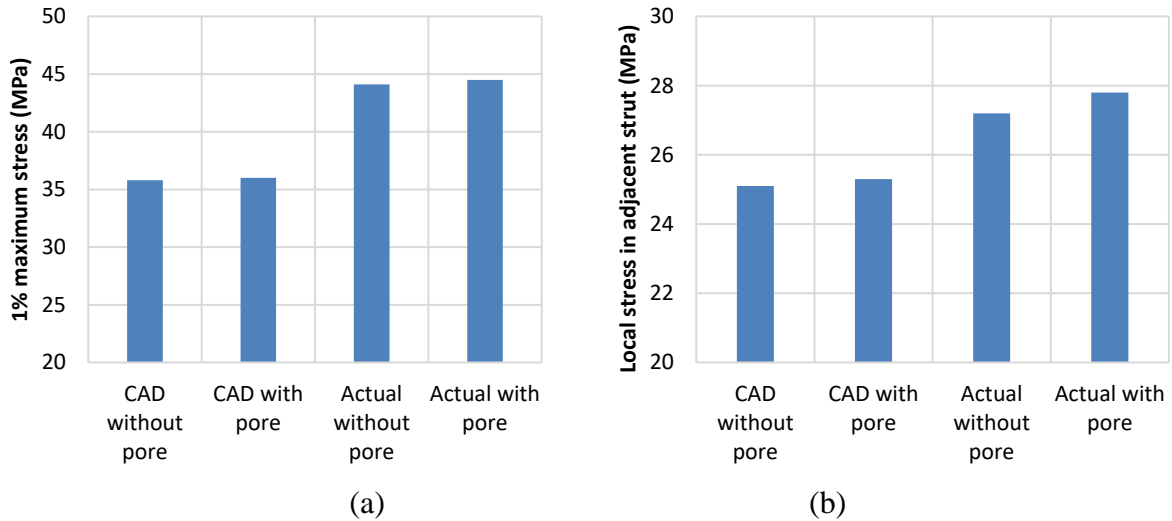


Figure 7: Simulation results comparing lattices: CAD design vs actual physical sample, with and without a spherical pore. The statistically averaged maximum 1% values (a) and the local stress in strut adjacent to strut with the pore (b) are shown. This shows the minimal influence of even a large pore space on compressive load stress.

Compression test results

Compression tests were done on 12 samples and the force at yielding is reported here, as a function of maximum pore size in the entire structure. All samples contained unintentional porosity. For the 4 control samples, these all had unintentional pores with the largest pore sizes in the size range 0.2 – 0.35 mm. The spherical and cubic pores all had diameters in the range 0.47–0.57 mm. As shown in Figure 8, despite the size of these pores, they have no influence on the yield force. This indicates that for the given surface roughness, even pores as large as 0.5 mm in a 0.75 mm diameter strut have no influence on the yield strength of the entire structure. In future work, it may be useful to image the crack paths where initial failure occurs, similar to that done in [12]. This would be useful especially for more complex lattices, and for improved understanding of failure mechanisms and the effect of pores on these mechanisms.

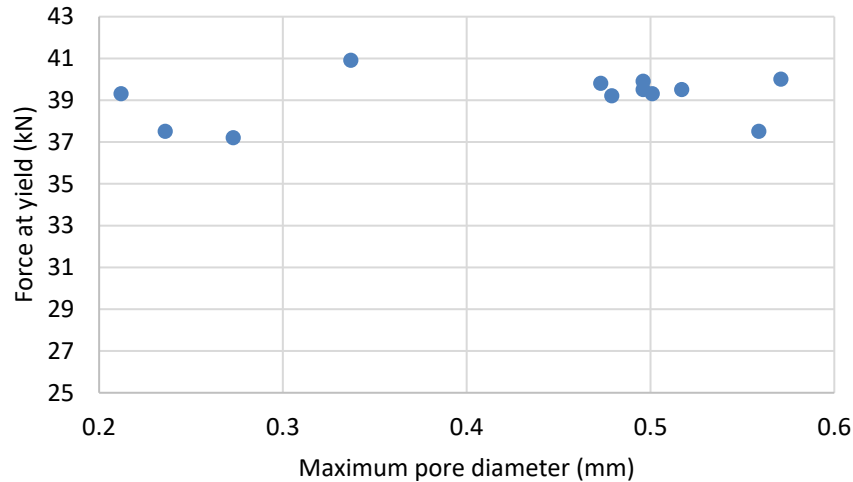


Figure 8: Yield force as a function of maximum pore size.

Conclusions

It was shown in this work, using numerical simulation and physical compression tests, that additively manufactured lattices may be produced for load bearing applications and the size of unintentionally produced pores will have minimal influence on the strength of the structure. From these results it is clear that not only does lattice design play a major role in the local stresses but also the nature of surface roughness of additive manufactured parts. It can be expected that reduction of stresses with less sharp corners in the lattice design, and less rough surface, will lead to stronger structures, and may be especially valuable for increasing fatigue life. Static compressive strength of a simple cubic lattice structure produced by LPBF seems to be independent of typical pores with sizes known to originate during the manufacturing process. This work indicates that lattices may be produced confidently despite large unintentional pore spaces (such as those produced in various LPBF processes) for static loading applications. The results presented are however limited to one lattice design, with one pore location. Different designs, different pore locations and combinations of numerous pores, and samples with different amounts of surface roughness/imperfections, may behave differently. Future work might extend this to encompass a wider range of possible conditions, in order to elucidate the true “effect of defect”. The results are however encouraging for the wider adoption of AM lattice designs in various applications, despite inherent defects occurring during production of such lattices.

Acknowledgements

Authors are grateful to the Centre for Rapid Prototyping and Manufacturing at Central University of Technology, Free State for manufacturing Ti6Al4V ELI samples.

References

- [1] X. P. Tan, Y. J. Tan, C. S. L. Chow, S. B. Tor, and W. Y. Yeong, “Metallic powder-bed based 3D printing of cellular scaffolds for orthopaedic implants: A state-of-the-art review on manufacturing, topological design, mechanical properties and biocompatibility,” *Mater.*

- Sci. Eng. C*, vol. 76, pp. 1328–1343, Jul. 2017.
- [2] X. Wang *et al.*, “Topological design and additive manufacturing of porous metals for bone scaffolds and orthopaedic implants: A review,” *Biomaterials*, vol. 83, pp. 127–41, Mar. 2016.
- [3] X.-Y. Zhang, G. Fang, and J. Zhou, “Additively Manufactured Scaffolds for Bone Tissue Engineering and the Prediction of their Mechanical Behavior: A Review,” *Materials (Basel)*, vol. 10, no. 1, p. 50, Jan. 2017.
- [4] L. E. Murr, “Open-cellular metal implant design and fabrication for biomechanical compatibility with bone using electron beam melting,” *J. Mech. Behav. Biomed. Mater.*, vol. 76, pp. 164–177, Dec. 2017.
- [5] L. Gibson and M. Ashby, “Cellular solids: structure and properties,” 1999.
- [6] M. Ashby, T. Evans, N. Fleck, and J. Hutchinson, *Metal foams: a design guide*. 2000.
- [7] J. Parthasarathy, B. Starly, S. Raman, and A. Christensen, “Mechanical evaluation of porous titanium (Ti6Al4V) structures with electron beam melting (EBM),” *J. Mech. Behav. Biomed. Mater.*, vol. 3, no. 3, pp. 249–259, Apr. 2010.
- [8] E. Sallica-Leva, A. L. Jardini, and J. B. Fogagnolo, “Microstructure and mechanical behavior of porous Ti–6Al–4V parts obtained by selective laser melting,” *J. Mech. Behav. Biomed. Mater.*, vol. 26, pp. 98–108, Oct. 2013.
- [9] H. Gong, K. Rafi, H. Gu, G. D. Janaki Ram, T. Starr, and B. Stucker, “Influence of defects on mechanical properties of Ti–6Al–4 V components produced by selective laser melting and electron beam melting,” *Mater. Des.*, vol. 86, pp. 545–554, Dec. 2015.
- [10] M. Smith, Z. Guan, and W. J. Cantwell, “Finite element modelling of the compressive response of lattice structures manufactured using the selective laser melting technique,” *Int. J. Mech. Sci.*, vol. 67, pp. 28–41, Feb. 2013.
- [11] H. D. Carlton *et al.*, “Mapping local deformation behavior in single cell metal lattice structures,” *Acta Mater.*, vol. 129, pp. 239–250, May 2017.
- [12] A. du Plessis, I. Yadroitsava, and I. Yadroitsev, “Ti6Al4V lightweight lattice structures manufactured by laser powder bed fusion for load-bearing applications,” *Opt. Laser Technol.*, vol. In press, 2018.
- [13] V. J. Challis, X. Xu, L. C. Zhang, A. P. Roberts, J. F. Grotowski, and T. B. Sercombe, “High specific strength and stiffness structures produced using selective laser melting,” *Mater. Des.*, vol. 63, pp. 783–788, Nov. 2014.
- [14] V. Weißmann, P. Drescher, R. Bader, H. Seitz, H. Hansmann, and N. Laufer, “Comparison of Single Ti6Al4V Struts Made Using Selective Laser Melting and Electron Beam Melting Subject to Part Orientation,” *Metals (Basel)*, vol. 7, no. 3, p. 91, Mar. 2017.
- [15] R. Hedayati, M. Sadighi, M. Mohammadi-Aghdam, and A. A. Zadpoor, “Mechanics of additively manufactured porous biomaterials based on the rhombicuboctahedron unit cell,” *J. Mech. Behav. Biomed. Mater.*, vol. 53, pp. 272–294, Jan. 2016.
- [16] V. Weißmann, J. Wieding, H. Hansmann, N. Laufer, A. Wolf, and R. Bader, “Specific Yielding of Selective Laser-Melted Ti6Al4V Open-Porous Scaffolds as a Function of Unit Cell Design and Dimensions,” *Metals (Basel)*, vol. 6, no. 7, p. 166, Jul. 2016.
- [17] I. Maskery, C. Tuck, R. D. Wildman, and R. I. M. Hague, “A COMPARATIVE FINITE ELEMENT STUDY OF CUBIC UNIT CELLS FOR SELECTIVE LASER MELTING,” in *Solid freeform fabrication*, 2014.
- [18] A. du Plessis, I. Yadroitsava, I. Yadroitsev, S. le Roux, and D. Blaine, “Numerical comparison of lattice unit cell designs for medical implants by additive manufacturing,” *Virtual Phys. Prototyp.*, pp. 1–16, Jun. 2018.

- [19] G. Campoli, M. S. Borleffs, S. Amin Yavari, R. Wauthle, H. Weinans, and A. A. Zadpoor, "Mechanical properties of open-cell metallic biomaterials manufactured using additive manufacturing," *Mater. Des.*, vol. 49, pp. 957–965, Aug. 2013.
- [20] P. Krakhmalev, G. Fredriksson, I. Yadroitsava, N. Kazantseva, A. Du Plessis, and I. Yadroitsev, "Deformation behavior and microstructure of Ti6Al4V manufactured by SLM," in *Physics Procedia*, 2016.
- [21] I. Yadroitsev, P. Krakhmalev, I. Yadroitsava, and A. Du Plessis, "Qualification of Ti6Al4V ELI Alloy Produced by Laser Powder Bed Fusion for Biomedical Applications," *JOM*.
- [22] S. Tammam-Williams, P. J. Withers, I. Todd, and P. B. Prangnell, "The Influence of Porosity on Fatigue Crack Initiation in Additively Manufactured Titanium Components," *Sci. Rep.*, vol. 7, no. 1, p. 7308, Dec. 2017.
- [23] A. du Plessis, I. Yadroitsev, I. Yadroitsava, and S. G. Le Roux, "X-Ray Microcomputed Tomography in Additive Manufacturing: A Review of the Current Technology and Applications," *3D Print. Addit. Manuf.*, 2018.
- [24] A. du Plessis *et al.*, "Prediction of mechanical performance of Ti6Al4V cast alloy based on microCT-based load simulation," *J. Alloys Compd.*, vol. 724, 2017.
- [25] J. Fieres, P. Schuman, and C. Reinhart, "Predicting failure in additively manufactured parts using X-ray computed tomography and simulation," *Procedia Eng. Press*.
- [26] A. du Plessis, C. Broeckhoven, I. Yadroitsev, I. Yadroitsava, and S. G. le Roux, "Analyzing nature's protective design: The glyptodont body armor," *J. Mech. Behav. Biomed. Mater.*, vol. 82, 2018.
- [27] A. du Plessis, S. G. le Roux, and A. Guelpa, "The CT Scanner Facility at Stellenbosch University: An open access X-ray computed tomography laboratory," *Nucl. Instruments Methods Phys. Res. Sect. B Beam Interact. with Mater. Atoms*, 2016.
- [28] A. du Plessis, I. Yadroitsev, I. Yadroitsava, and S. le Roux, "X-ray micro computed tomography in additive manufacturing: a review of the current technology and applications," *3D Print. Addit. Manuf.*, vol. 0, no. 0.
- [29] A. du Plessis, S. G. le Roux, G. Booyen, and J. Els, "Quality Control of a Laser Additive Manufactured Medical Implant by X-Ray Tomography," *3D Print. Addit. Manuf.*, 2016.
- [30] A. du Plessis, S. G. le Roux, and F. Steyn, "X-Ray Computed Tomography of Consumer-Grade 3D-Printed Parts," *3D Print. Addit. Manuf.*, vol. 2, no. 4, pp. 190–195, Dec. 2015.
- [31] A. du Plessis, C. Broeckhoven, A. Guelpa, and S. G. le Roux, "Laboratory x-ray micro-computed tomography: A user guideline for biological samples," *Gigascience*, vol. 6, no. 6, 2017.